Progress in Nuclear Energy 96 (2017) 118–132

Contents lists available at ScienceDirect

Progress in Nuclear Energy

journal homepage: www.elsevier.com/locate/pnucene

A two-dimensional experimental investigation on debris bed formation behavior

Shaopeng Lin, Songbai Cheng*, Guangyu Jiang, Ziyi Pan, Hantao Lin, Shixian Wang, Li Wang, Xiaoying Zhang, Biao Wang

Sino-French Institute of Nuclear Engineering & Technology, Sun Yat-Sen University, Tang-Jia-Wan, Zhuhai City, Guangdong Province, 519-082, PR China

A R T I C L E I N F O

Article history:
Received 9 June 2016
Received in revised form
20 August 2016
Accepted 28 December 2016
Available online 31 December 2016

Keywords:
Sodium-cooled fast reactor
Core disruptive accident
Debris bed formation
Experimental study

A B S T R A C T

Studies on debris bed formation behavior are of crucial importance for the improved evaluation of Core Disruptive Accidents (CDA) that could occur for Sodium-cooled Fast Reactors (SFR). In this work, to clarify the mechanisms underlying this behavior, a series of experiments was performed by discharging solid particles into two-dimensional rectangular water pools. To obtain a comprehensive understanding, various experimental parameters, including particle size (0.256~8 mm), particle density (glass, alumina, zirconia, steel and lead), particle shape (spherical and irregularly-shaped), water depth (0–60 cm), particle release pipe diameter (10–30 mm), particle release height (110–130 cm) as well as the gap thickness of water tank (30–60 mm), were varied. It is found that due to the different interaction mechanisms between solid particles and water pool, four kinds of regimes, termed respectively as the particle-suspension regime, the pool-convection dominant regime, the transitional regime and the particle-inertial dominant regime, are identified. The performed analyses in this work also suggest that under present experimental conditions, the particle size, particle density, particle shape, particle release pipe diameter and water depth are observable to have remarkable impact on the above regimes, while the role of particle release height and gap thickness of water tank seems to be less prominent. Knowledge and data from this work might be utilized for the improved design of core catcher as well as analyses and verifications of SFR severe accident analysis codes in China in the future.

1. Introduction

The disaster in March 2011 at the Fukushima Dai-Ichi nuclear power plant in Japan has caused many people to realize that severe accidents, including the Core Disruptive Accidents (CDAs), might occur, even if their probability is extremely lower (Cheng et al., 2014a, 2015). During a postulated CDA in a Sodium-cooled Fast Reactor (SFR), possibly as a consequence of rapid quenching and fragmentation of core materials, a multiphase flow system can form that could be composed of a mixture of liquid sodium, molten fuel, molten structure, refrozen fuel, solid fuel pellets, fission gas, fuel vapor, and other materials (Tentner et al., 2010). A deposition of this system will lead to the formation of debris beds over the core-support structure and/or in the lower inlet plenum of the reactor vessel, as depicted in Fig. 1 (Zhang et al., 2010, 2011).

To prevent the penetration of the reactor vessel by molten fuel, and distribute molten fuel or core debris formed in a CDA into non-critical configurations, in-vessel retention devices (e.g. the core catcher) are used in some SFR designs (Tentner et al., 2010; Waltar and Reynolds, 1981). Although the detailed structure of the core catcher (e.g. single-layer or multi-layer) might be different depending on the reactor-type in different countries (Nakai et al., 2010; Ren, 2015; Vasilyev et al., 2013), it is expected that during a hypothetical CDA, after being quenched and fragmented into fuel debris in the lower plenum region, discharged molten fuel should be accumulated on the layers of the core catcher. To stably remove the decay heat generated from the debris bed on the core catcher, thus, the size, retention capability and structure of the catcher should be carefully designed.

Unfortunately, over the past decades, although extensive studies on debris bed hydrodynamics and heat transfer were performed (Cheng et al., 2010), most of them generally assumed that the upper surface of debris bed is level. Noting the importance of debris-bed geometry (e.g. height) in the heat removal capability, recently by

* Corresponding author.
E-mail address: chengsb3@mail.sysu.edu.cn (S. Cheng).

http://dx.doi.org/10.1016/j.pnucene.2016.12.008
0149-1970/

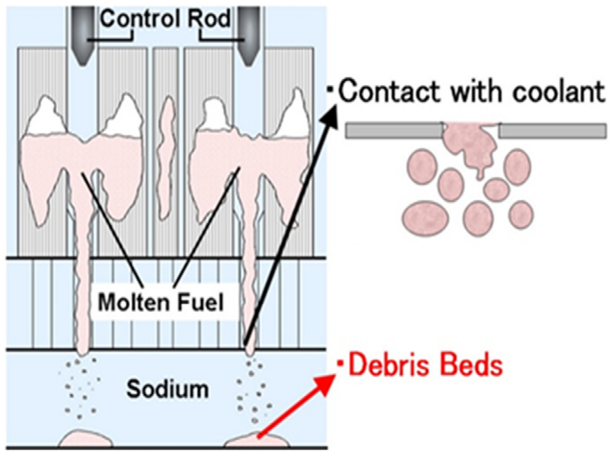

Fig. 1. Debris bed profile.

assuming that a conically-shaped debris bed might be initially formed, Cheng et al. (2011a, b; 2013a, b, c; 2014b, c) performed several series of experiments on the so-called debris bed self-leveling behavior (see Fig. 2). Overall, as illustrated in Fig. 3, their experiments can be generally divided into two categories, namely the macroscopic leveling experiments and microscopic flow-regime investigations. Due to the nontransparency of particle beds, the macroscopic leveling experiments were mainly conducted with the purpose to clarify the overall characteristics of leveling (Cheng et al., 2013a, b; 2014b, c), namely the role of experimental parameters (such as particle properties and bubbling rate) on the leveling onset and evolution. As for the microscopic flow-regime series (Cheng et al., 2010, 2011a, 2013a), which also consists of several well-organized tests performed at various bubbling conditions (as shown in Fig. 3), was specifically carried out to ascertain the flow characteristics within particle beds, thus providing convincible visual evidence (esp. bubble-particle interaction) for supporting the overall understandings. It has been confirmed that by combining the knowledge from flow-regime investigations the observed overall leveling characteristics can be understood more effectively (Cheng et al., 2013a).

In this paper, motivated by acquiring some evidence to verify whether the initial particle bed formed is conical or not, a series of experiments on the debris bed formation behavior is conducted within a variety of conditions including much difference in particle size (0.256~8 mm), particle density (glass, alumina, zirconia, steel and lead), particle shape (spherical and irregularly-shaped), water depth (0–60 cm), particle release pipe diameter (10–30 mm), particle release height (110–130 cm) and the gap thickness of water tank (30–60 mm). The experimental apparatus and procedures are described in Section 2, while the obtained results and their interpretations are discussed in detail in Section 3. Knowledge and

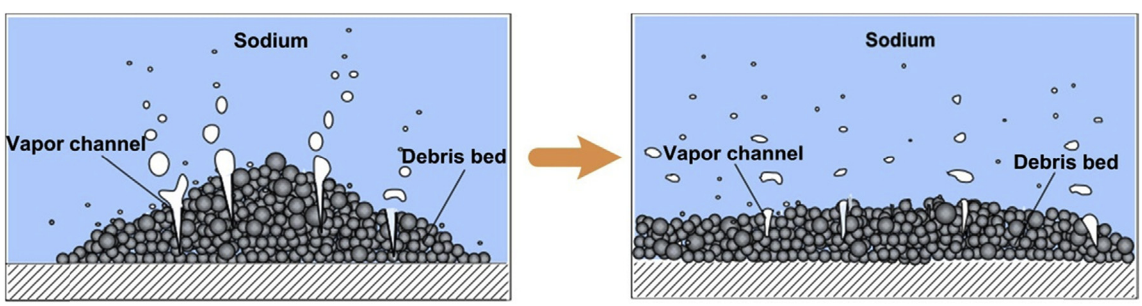

Fig. 2. Debris bed self-leveling behavior.

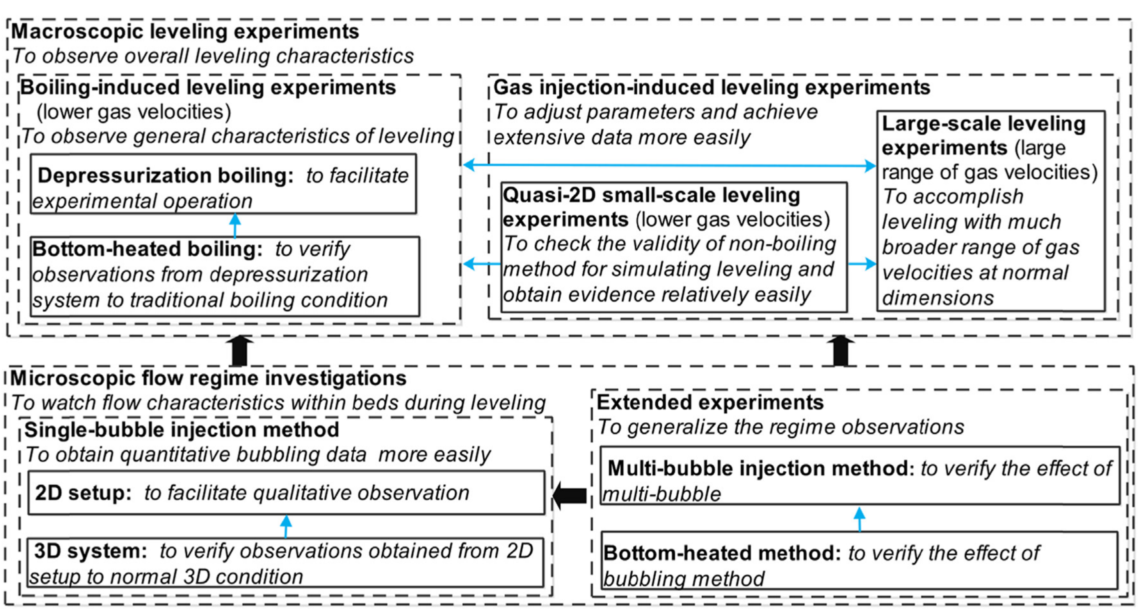

Fig. 3. Constitution of leveling-related experiments performed by Cheng et al. (2013a, 2014b). (a) Schematic view of experimental system (b) Detailed view of the main apparatus.

data from this work might be utilized for the improved design of core catcher as well as verifications of computer models (e.g. the particle-liquid interaction model) developed in Chinese SFR severe accident analysis codes in the future.

2. Experimental apparatus and procedures

Fig. 4 (a) depicts the schematic diagram of the whole experimental system used in this work, while Fig. 4(b) further shows a detailed view of the main apparatus. To facilitate the visual observation and quantitative measurement, two-dimensional (2D) viewing tanks made of transparent acrylic resin with the dimensions of 1000 mm in height, 700 mm in width and 30–60 mm in gap thickness were utilized. Water, which was poured into the tank from the top of the viewing tank, is employed to simulate the coolant. Before the commencement of each experimental run, water-depth was adjusted to target values. At the bottom of the viewing tank, a drain valve allowing water and solid particles to drain out of the tank after experiments is designed.

To simulate the fuel debris, five kinds of particles (namely glass, alumina, zirconia, steel and lead) with different sizes and shapes were used, the properties of which are listed in Table 1. It is believed that such a range of physical properties (for example, the particle size and density) might be possibly broad to cover the entire range

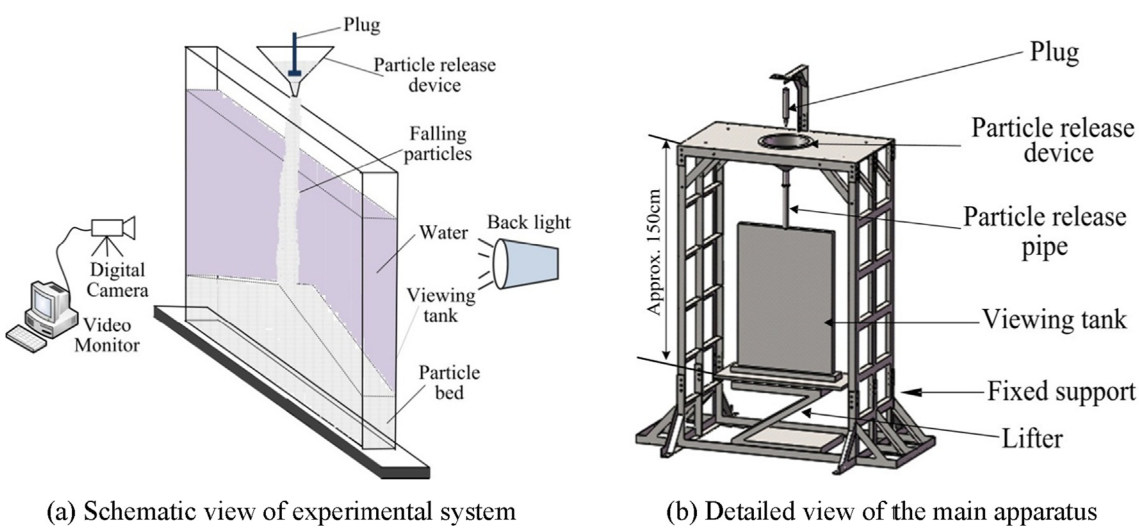

Fig. 4. Experimental setup used in this work.

Table 1
Physical properties of solid particles.

Material	Density (kg/m^3)	Size (mm)	Shape	Terminal velocity (10^{-2} m/s) [a]
Glass	2600	0.25	Sphere	3.32
		0.5		7.51
		1		15.29
		2		27.34
		2.5		32.21
		4		44.55
		6		57.31
		8		66.05
Alumina	3600	0.5	Sphere	10.54
		0.8		16.95
		1		20.89
		2		36.28
		4		58.22
		6		73.26
		0.5–0.6	Non-sphere	10.54[b]
		0.9–1.0		19.91[b]
		1.5–1.6		29.30[b]
Zirconia	6000	0.4	Sphere	13.04
		2		52.55
		4		82.52
Steel	7900	0.6	Sphere	24.31
		1		38.13
		2		63.07
		4		97.44
		6		117.98
Lead	11 340	2	Sphere	79.13
		4		119.01
		6		142.82

[a] Estimated in water using Stokes's Law for small particles, and Heywood Tables for larger particles (Fan and Zhu, 1998).
[b] Estimated based on the volume-equivalent diameter without considering the particle-shape effect (Cheng et al., 2014c).

of physical properties of actual debris generated during CDAs of a typical SFR (e.g. mean debris size of several hundreds of microns and a maximum density of fuel (MOX) pellets up to about 11 g/cm^3) (Cheng et al., 2013a; IAEA, 2016).

Before the start of each experimental run, a fixed volume (10 L) of solid particles is carefully weighed and delivered into the particle release device which is actually a conical funnel made of stainless steel. To avoid the potential dispersion of solid particles out of the water tank during their free-falling, cylindrical pipes with appropriate lengths and inner diameters (10–30 mm) were connected at the bottom of the particle release device. By pulling the plug upwards with a string, particles initially accumulated in the funnel will be released and fall into the water tank due to the gravity. The whole experimental process is recorded by a video camera which can record tens of frames per second (fps). To obtain a high-quality recording, for most cases back-lighting was applied along a vertical distance. By using image analysis software, stills extracted from the video recording after experiments were used for further qualitative observation and quantitative measurement.

To obtain the general characteristics of debris bed formation behavior, a variety of experimental parameters including particle size (d_p), particle density (ρ_p), particle shape, water depth (H_w), particle release pipe diameter (D_{pipe}), particle release height (H_p) as well as the gap thickness of water tank (W_{tank}), were taken. Table 2 summarizes the specific conditions of all experimental runs currently performed.

3. Experimental analyses and discussion

3.1. Identification of regimes

Based on the observations from experimental process as well as the stills recorded, characteristics of the debris bed formation behavior were elaborately analyzed and compared for all the runs listed in Table 2. It is found that due to the different interaction mechanisms observed between solid particles and water pool, four kinds of regimes, termed respectively as the particle-suspension regime, the pool-convection dominant regime, the transitional

Table 2
Experimental parameters.

Case no.	Material	d_p (mm)	Shape	H_w (cm)	D_{pipe} (mm)	H_p (cm)	W_{tank} (mm)	Release time (s) [a]	Regime identification [b]
1	Glass	0.25	Sphere	60	30	110	60	29	I
2		0.5						29	II
3		1						36	II
4		2						39	III
5		2.5						46	IV
6		4						55	IV
7		6						71	IV
8		8						100	IV
9	Alumina	0.5	Sphere					29	II
10							45	30	II
11							30	29	II
12						120	60	29	II
13						130		29	II
14				45		110		29	II
15				25				31	III
16				0				30	IV
17				60	20			79	III
18					10			460	IV
19		0.8			30			32	III
20		1						34	III
21		2						38	IV
22					20			86	IV
23					10			617	IV
24		4			30			55	IV
25		6						71	IV
26							45	75	IV
27							30	73	IV
28						120	60	74	IV
29						130		73	IV
30				30		110		72	IV
31		0.5–0.6	Non-sphere	60				38	III
32		0.9–1.0						41	III
33		1.5–1.6						44	IV
34	Zirconia	0.4	Sphere					30	II
35		2						38	IV
36		4						50	IV
37	Steel	0.6						34	IV
38		1						34	IV
39		2						39	IV
40		4						53	IV
41		6						64	IV
42	Lead	2						37	IV
43		4						50	IV
44		6						67	IV

[a] The particle release time is defined as the total time that all 10 L particles need to release, namely the time span between the first particle and last particle flowing out of the particle release pipe.

[b] In this column, the numbers I, II, III and IV represent respectively the particle-suspension regime, the pool-convection dominant regime, the transitional regime and the particle-inertial dominant regime.

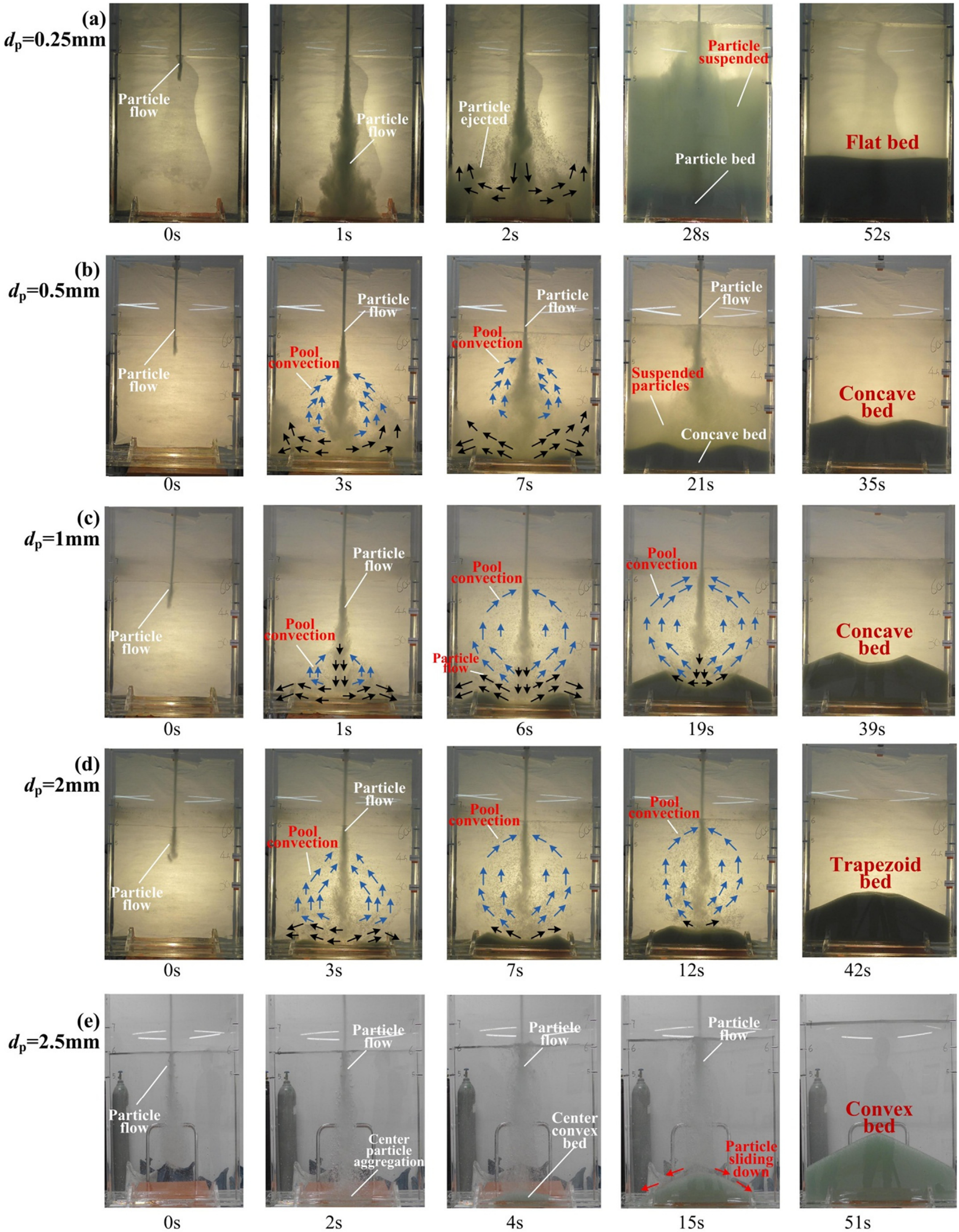

Fig. 5. Transient debris bed formation behavior. (Glass beads, $H_w = 60$ cm, $D_{pipe} = 30$ mm, $H_p = 110$ cm, $W_{tank} = 60$ mm).

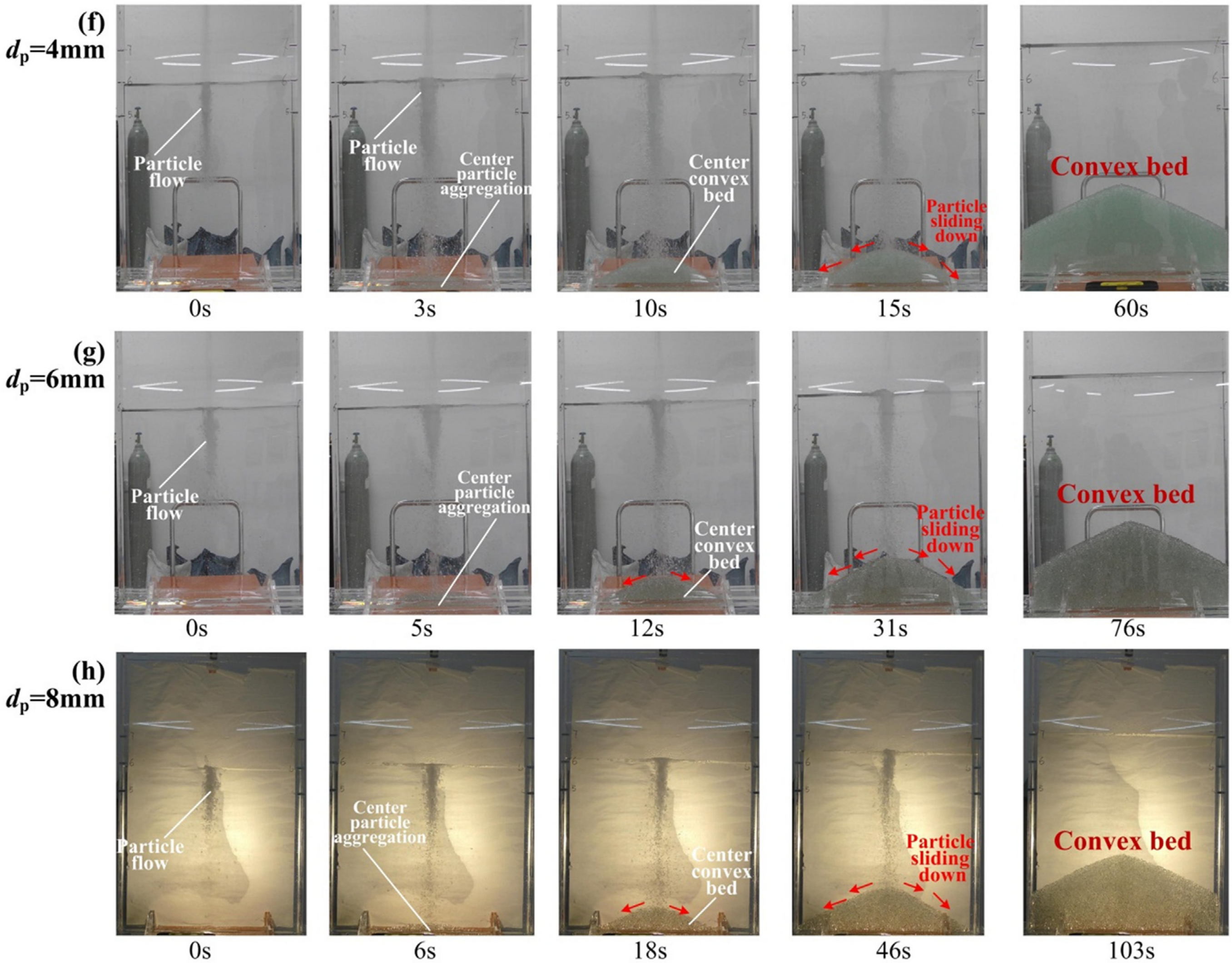

Fig. 5. (*continued*).

regime and the particle-inertial dominant regime, could be identified. A summary of the regime identification is given in Table 2. Since from our previous experimental studies on the debris bed self-leveling behavior (Cheng et al., 2011a, 2013a), it has been well understood that compared to other parameters (e.g. particle density), the particle size seems to play a more evident role in determining the transition of bubbling behaviors, therefore in this Section, experimental cases No. 1–8 which were conducted using glass beads with a larger range of sizes (0.25–8 mm) are selected for interpreting the characteristics of each regime:

(1) *Particle-suspension regime.* For glass beads, this regime could be observed with $d_p \le 0.25mm$. As shown in Fig. 5(a), particles in this regime, due to their lighter weight, are quite susceptible to being ejected by the particle flow. The ejected particles tend to be suspended comparatively uniformly around the water pool and sediment gradually on the pool bottom, especially after the completion of particle release. Since the suspended particles are distributed very uniformly, a final *flat bed* is formed.
(2) *Pool-convection dominant regime.* For glass beads, this regime exists with $0.25mm < d_p \le 1mm$. As shown in Fig. 5(b) and (c), forced by the continuous particle flow released into the pool, in this regime evident pool convection is observable. However, since compared to the particle-suspension regime, the mass of a single particle is much increased; it seems that in this regime particles become quite difficult to be suspended, particularly in Fig. 5(c) with a size up to around 1 mm. It is found that at the early stage, because of the violent pool convection, particles are driven away and form two mounds at the bottom. With the ongoing of particle transporting, more and more particles are observable to be accumulated, leading to the formation of a final *concave bed* with two apexes.
(3) *Transitional regime.* For glass beads, this regime is observed with $1mm < d_p \le 2mm$. As shown in Fig. 5(d), similar to the pool-convection dominant regime, at the beginning two mounds at the bottom of water tank are formed. However, possibly due to an increased inertial of a single particle as well as the particle-particle frictions (as compared to the frictions between particles and the tank bottom), particles in this regime are observed to become more difficult to be pushed away by the subsequent pool convection. As a result, more and more particles will sediment around the center of the tank, leading to the formation of a final *quasi-trapezoid bed.*

(4) *Particle-inertial dominant regime.* For glass beads, this regime is found to exist with $d_p > 2mm$. It is imaginable that, due to a much larger size, the probability of particle-particle collisions within the particle-release device as well as the connecting pipe is supposed to be largely enhanced, thereby leading to quite diminished particle release rate (see the measured data of particle release time in Table 2). As a result, unlike the above regimes, as shown in Fig. 5(e)~(h), in this regime evident pool convection seems difficult to be formed. At the beginning, particles tend to form a single bed at the bottom center. With the ongoing of particle delivering, the latter particles are observed to slide down the slope, resulting in a final *convex bed.*

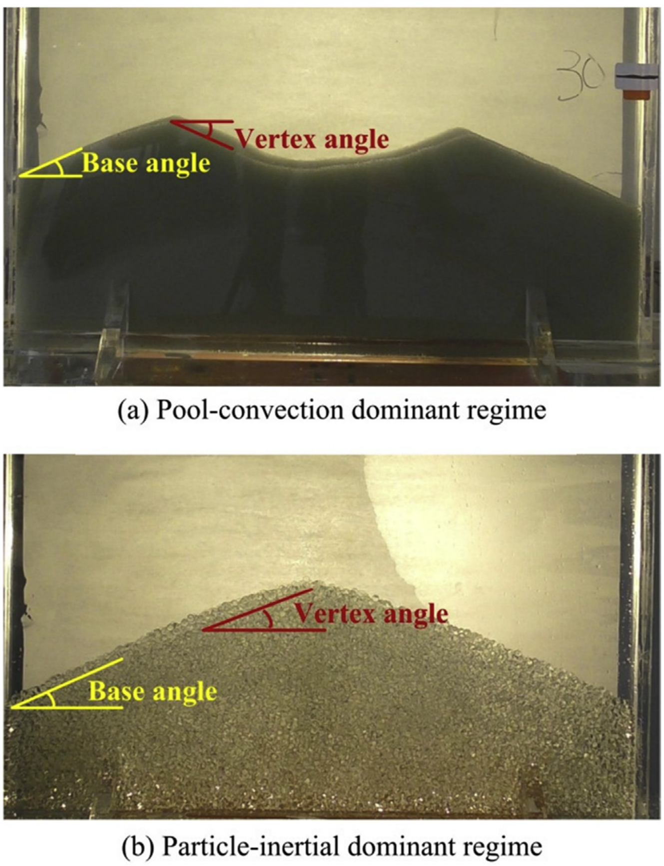

Fig. 6. Diagram of defined angles. (a) Base angle (b) Vertex angle.

3.2. Analyses of experimental parameters

As indicated in Section 3.1, the final bed geometry (flat, concave, quasi-trapezoid or convex) is a key indicator to distinguish different regimes. However, motivated to acquire more information for understanding the debris bed formation behavior, in addition to the final bed geometry, in this Section two additional quantities, namely the base angle and vertex angle, are also defined (see Fig. 6). It is evident that according to their definitions, for all regimes mentioned above, a non-negative value of base angle should be obtained. As for the vertex angle, a minus value should be attained for the pool-convection dominant regime, which is different from others.

3.2.1. Effect of particle size

Fig. 7 shows the variation with particle size of measured angles for glass beads. From Fig. 7(a), it can be clearly seen that with the increasing of particle size, the base angle tends to increase initially (from 0°) and then approach constant values. Actually, it should not be surprising since as mentioned-above, under present experimental conditions, as particle size increases from 0.25 mm to 8 mm, the transition of 4 regimes occurs. In the particle-suspension regime (e.g. $d_p \leq 0.25mm$), a flat bed, namely a base angle of around zero, is attained; while for the pool-convection dominant regime (e.g. $0.5mm \leq d_p \leq 1mm$), a concave bed with two apexes is obtained, thereby resulting in increased base angle. As for the transitional and particle-inertial dominant regimes (e.g. $d_p \geq 2.5mm$), as pointed-above, the base angle is governed by the particle sliding process (see Fig. 5(e)~(h)), in which a critical angle (or the angle of repose) tends to appear (Barabasi et al., 1999).

From Fig. 7(b), it is seen that with increasing particle size, the vertex angle is firstly decreasing (from zero), then increases and finally tends to approach constant values, which evidently should be caused by the transition of regimes as well. According to the definition shown in Fig. 6, it is easily seen that for both the particle-suspension regime and the transitional regime, a vertex angle of around zero should be obtained. The reason why the absolute value of vertex angle in the case using 0.5 mm glass beads is smaller than the case using 1 mm particles is because in such a case the particle-

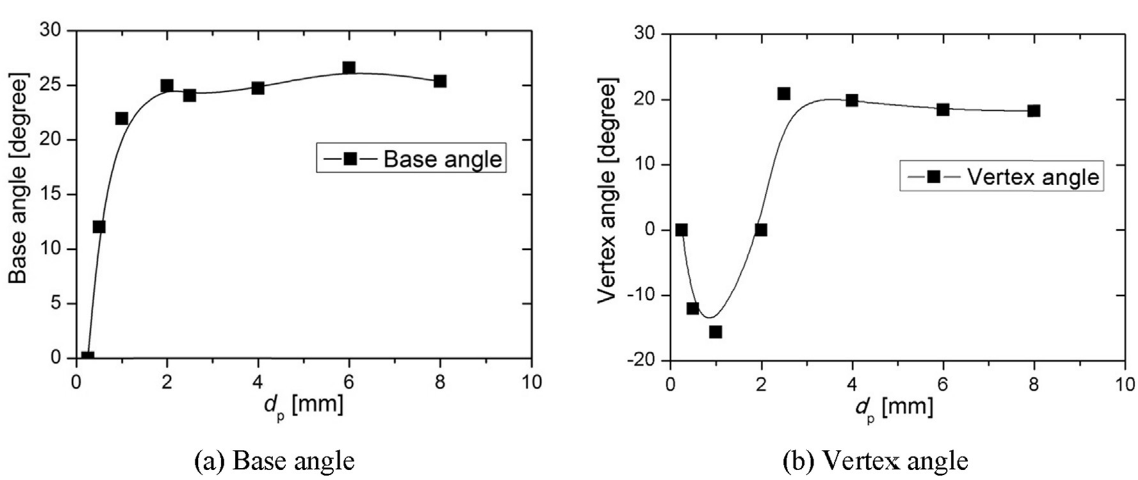

Fig. 7. Effect of particle size on measured angles. (Glass beads, H_w = 60 cm, D_{pipe} = 30 mm, H_p =110 cm, W_{tank} = 60 mm).

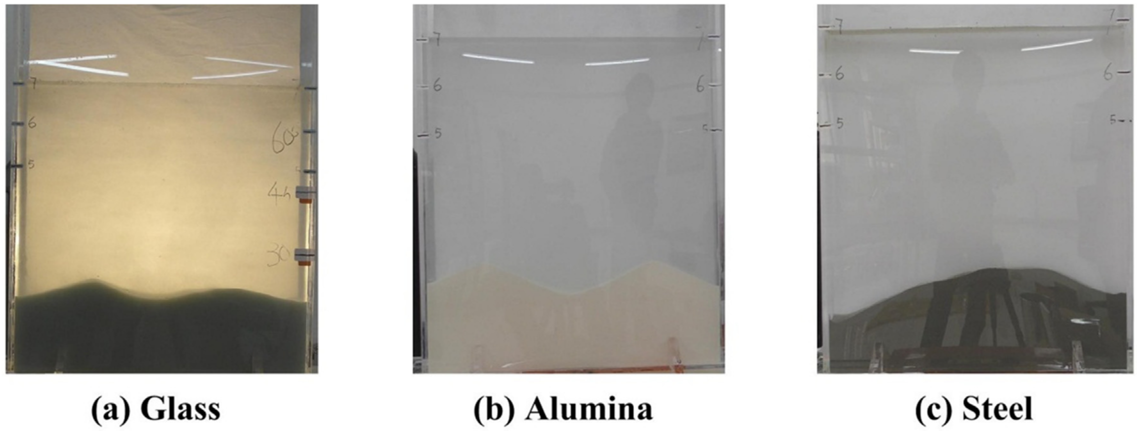

Fig. 8. Effect of particle density on final bed geometry for small particles. (Spherical particles, d_p = 0.5–0.6 mm, H_w = 60 cm, D_{pipe} = 30 mm, H_p = 110 cm, W_{tank} = 60 mm).

suspension effect remains to some degree, although as compared to the particle-suspension regime its intensity has been much diminished (see Fig. 5(b)). By making comparisons between Fig. 7(a) and (b), one more point that can be understood is that for the particle-inertial dominant regime, the base angle seems to be comparatively larger than the vertex angle (about 5°). Again, it should be reasonable since the collisions from the falling particles is supposed to have a certain compressing impact on the vertex region of particle beds.

3.2.2. Effect of particle density

Since the mechanisms underlying different regimes are quite

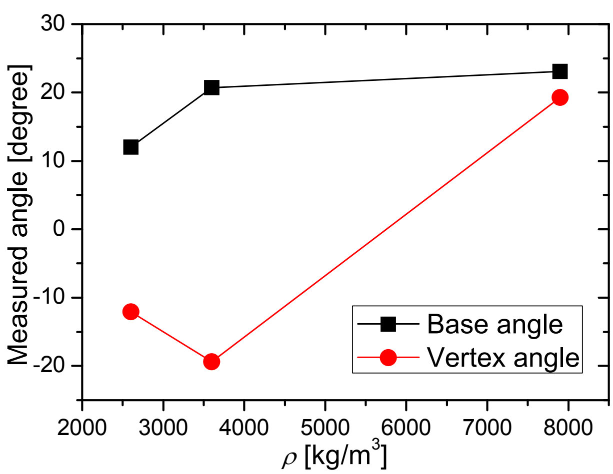

Fig. 9. Effect of particle density on measured angles for small particles. (Spherical particles, d_p = 0.5–0.6 mm, H_w = 60 cm, D_{pipe} = 30 mm, H_p =110 cm, W_{tank} = 60 mm).

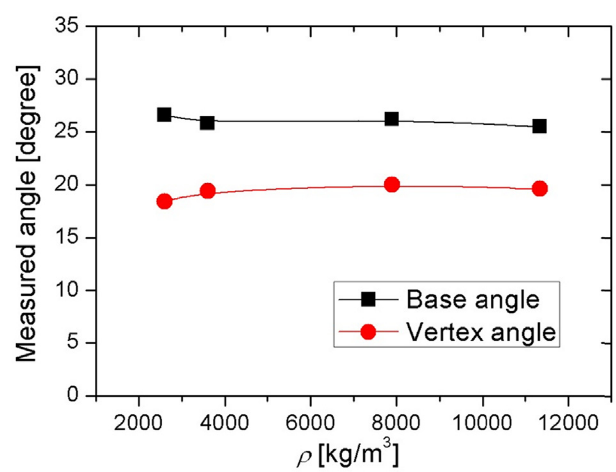

Fig. 11. Effect of particle density on measured angles for big particles. (Spherical particles, d_p = 6 mm, H_w = 60 cm, D_{pipe} = 30 mm, H_p =110 cm, W_{tank} = 60 mm).

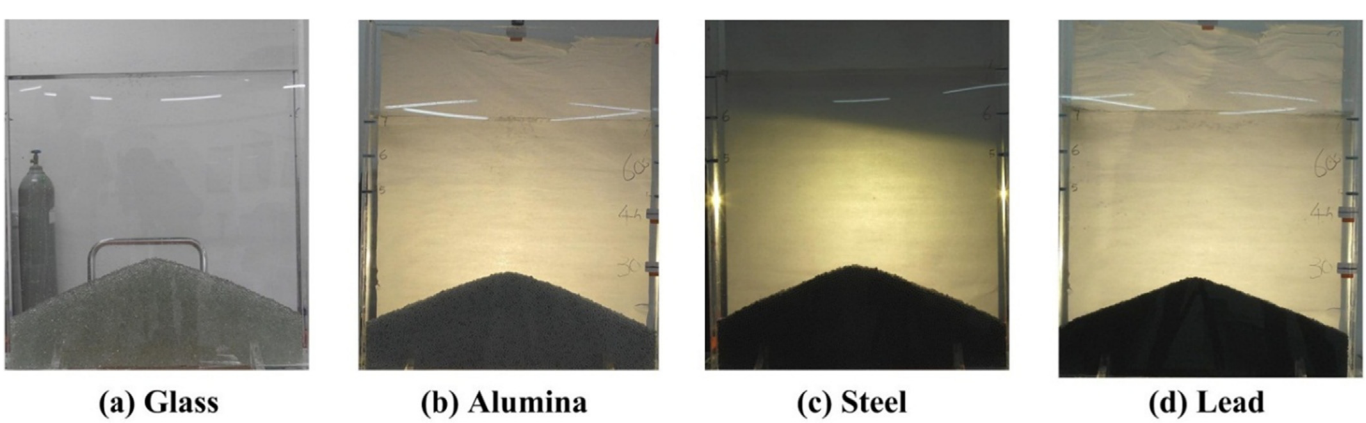

Fig. 10. Effect of particle density on final bed geometry for big particles. (Spherical particles, d_p = 6 mm, H_w = 60 cm, D_{pipe} = 30 mm, H_p = 110 cm, W_{tank} = 60 mm).

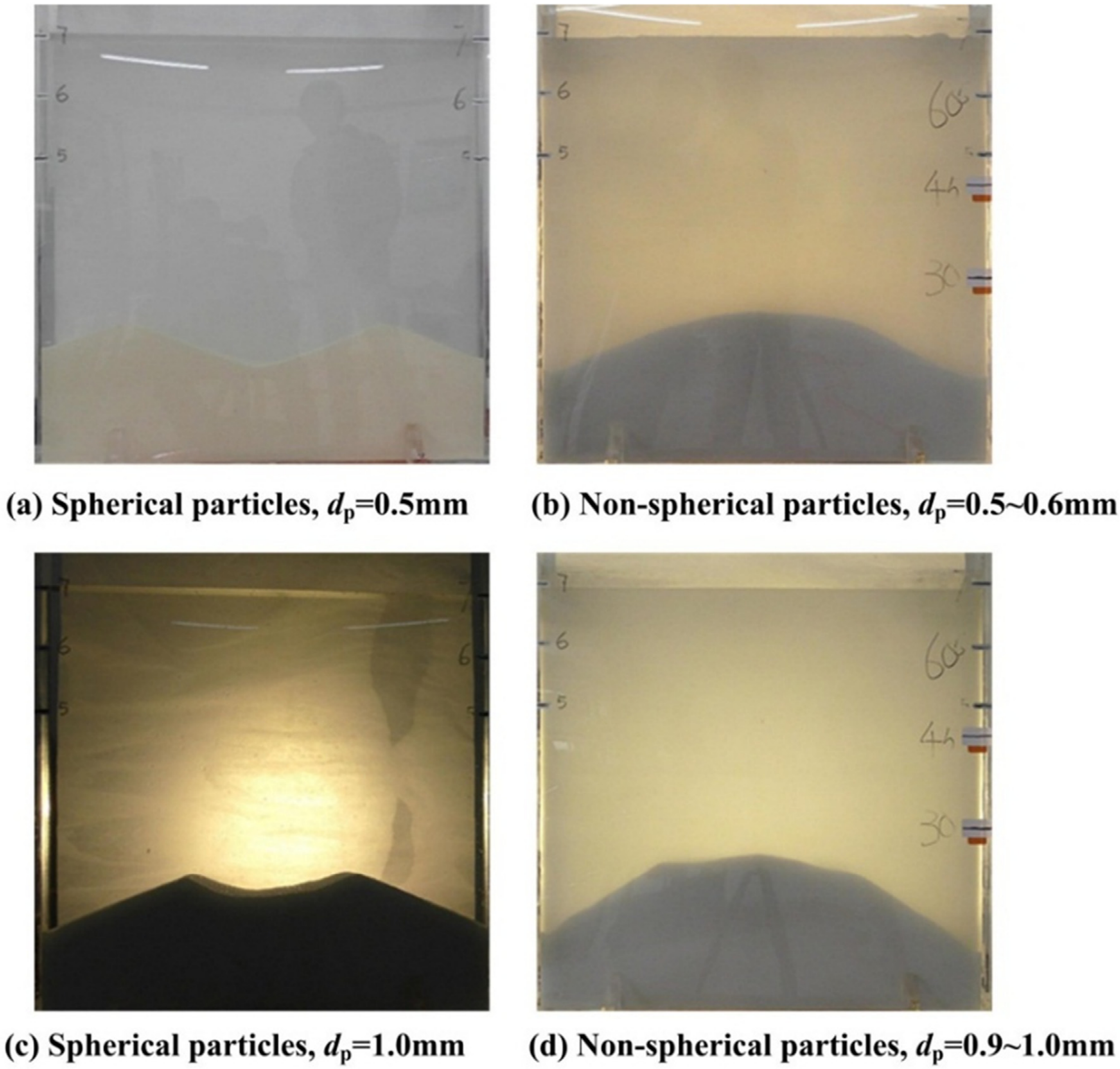

Fig. 12. Effect of particle shape on final bed geometry. (Alumina particles, H_w = 60 cm, D_{pipe} = 30 mm, H_p = 110 cm, W_{tank} = 60 mm).

different, from this part comparative analyses will be made according to the two main regimes, namely the pool-convection dominant regime (small particles) and the particle-inertial dominant regime (big particles), respectively.

Figs. 8 and 9 depict respectively the effect of particle density on final bed geometry and measured angles for around 0.5 mm-sized small particles. From Fig. 8, it is clear that as particle density increases, the observed regimes have been changed from the pool-convection dominant regime (concave bed) to the particle-inertial dominant regime (convex bed). Evidently, the measured angles in Fig. 9 can support this point very well. In addition, from Fig. 9 we may further find that the measured absolute values of base angle and vertex angle in the case using alumina particles are relatively larger than the case using glass beads, which again should be owing to the much suppressed effect of particle-suspension as particle density increases.

Figs. 10 and 11 illustrate respectively the effect of particle density on final bed geometry and measured angles for larger 6 mm-sized particles. From Fig. 10, it is seen that no transition of regimes has occurred, even if the particle density is much increased. In addition, from Fig. 11, we may further find that both the base angle and vertex angle are confirmable to be varied within a rather limited range. The above points can be well understood since as aforementioned, the mass of 6 mm glass beads is verified to be already large enough to enter the particle-inertial dominant regime.

3.2.3. Effect of particle shape

The effect of particle shape on final bed geometry for both 0.5 mm and 1 mm alumina particles are shown in Fig. 12. It is found that when the particle shape changes from sphere to non-sphere (or more accurately we call it “irregularly-shaped”), for both sizes, the transition of regimes is observable to occur. Again, it should not be surprising since as confirmed in our previous studies regarding the debris bed self-leveling behavior (Cheng et al., 2014c), compared to the cases using spherical particles, in the cases using non-spherical particles additional particle-particle collisions and frictions caused by the shape-related parameters (such as roughness and eccentricity) should exist, which inevitably will play an enhanced role in inhibiting the pool convection to act.

Another finding that can be understood from Fig. 12 is that although both the two cases using non-spherical particles might be classified into the transitional regime, the final bed geometry shown in Fig. 12(b) seems to be more close to the particle-inertial dominant regime, even if the particle size is comparatively smaller, which may indicate that in such a case the effective sphericity of non-spherical particles, as compared to the case shown in Fig. 12(d), should be much lower (or closer to 0). For this reason, a new facility measuring the effective sphericity of irregularly-shaped particles by back-calculation of the Ergun Equation is being developed at the Sun Yat-sen University (Cheng et al., 2014c). We believe, such a measured sphericity, is expectable to be quite useful for our future empirical-model studies on the debris bed formation behavior.

Based on the mechanisms analyzed above, it is imaginable that for the experimental cases using big-sized non-spherical particles (such as 6 mm), the particle-inertial dominant regime is deemed to occur under present conditions, although currently we are unable to perform such investigations due to the shortage of larger non-spherical particles.

3.2.4. Effect of water depth

The effect of water depth on the final bed geometry for smaller 0.5 mm alumina particles is shown in Fig. 13. Obviously, with the decreasing of water depth, the transition of regimes, even from the pool-convection dominant regime to the particle-inertial dominant regime, has occurred, which might be explained by the fact that, as illustrated in Fig. 14, higher water depth seems to promote the pool convection. Again, this finding is consistent with our previous studies regarding the debris bed self-leveling behavior in which nitrogen gas was injected into a water pool for simulating the decay-heat-induced coolant boiling (Cheng et al., 2013a, b). By making quantitative comparisons between Fig. 13(b), (c) and (d), it can be further recognized that because of the less-violent pool convection at lower water depths, both the measured vertex angle and apex distance are decreasing.

Fig. 15 shows the effect of water depth on the final bed geometry for larger 6 mm alumina particles. It is evident that no significant changes of final bed geometry are observable. This might be due to fact that for the case with a water depth of 60 cm, the influence of pool convection, as noted in Section 3.1, has been already sufficiently weak. In addition, it might be also judged that the static pressure of water pool seems to be limited.

3.2.5. Effect of particle release pipe diameter

The effect of particle release pipe diameter on the final bed geometry for smaller 0.5 mm alumina particles is shown in Fig. 16. Again, it is seen that with decreasing the pipe diameter, the observed regimes transit from the initial pool-convection dominant regime to the transitional regime and finally enter into the particle-inertial dominant regime. As depicted in Fig. 17, it is evident that compared to the case with a D_{pipe} of 30 mm, for the case shown in Fig. 17(a) the pool convection is observable to be much diminished. By checking the column "Release time" in Table 2, we can find that in such a case the particle release time is about 16 times (460/29) longer, even if its pipe diameter is just 1/3 times narrower. Therefore, we can guess that in the case with a pipe diameter of around 10 mm, the resistance from the pipe (e.g. frictions and collisions) is significantly strengthened (not just in a linear or quadratic proportion to D_{pipe}), thereby leading to much reduced particle release

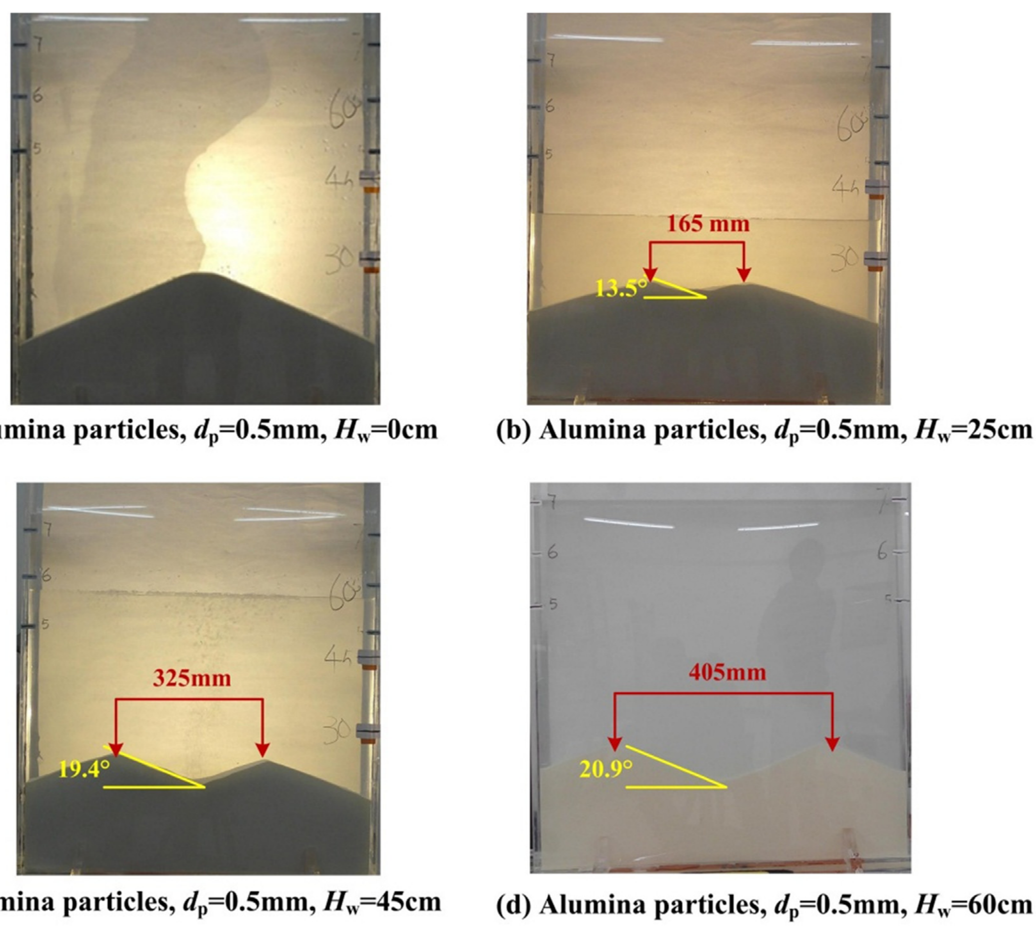

(a) Alumina particles, d_p=0.5mm, H_w=0cm

(b) Alumina particles, d_p=0.5mm, H_w=25cm

(c) Alumina particles, d_p=0.5mm, H_w=45cm

(d) Alumina particles, d_p=0.5mm, H_w=60cm

Fig. 13. Effect of water depth on final bed geometry (small particles). (Alumina beads, D_{pipe} = 30 mm, H_p = 110 cm, W_{tank} = 60 mm).

rate and less prominence of pool convection.

Although for the particle-inertial dominant regime it might be more preferable to perform comparative analyses using larger 6 mm particles, through several trial tests with a pipe diameter of around 10 mm, it is found that such larger particles become much easier to block the releasing pipe or even interrupt the particle delivering completely. For this reason, here the medium-sized 2 mm particles are employed for analyses. As shown in Fig. 18, one may find that with decreasing D_{pipe}, no remarkable change of final bed geometry has occurred, which might be due to the fact that for the experimental case with D_{pipe} of 30 mm, the pool convection has been already observed to be sufficiently weak (leading

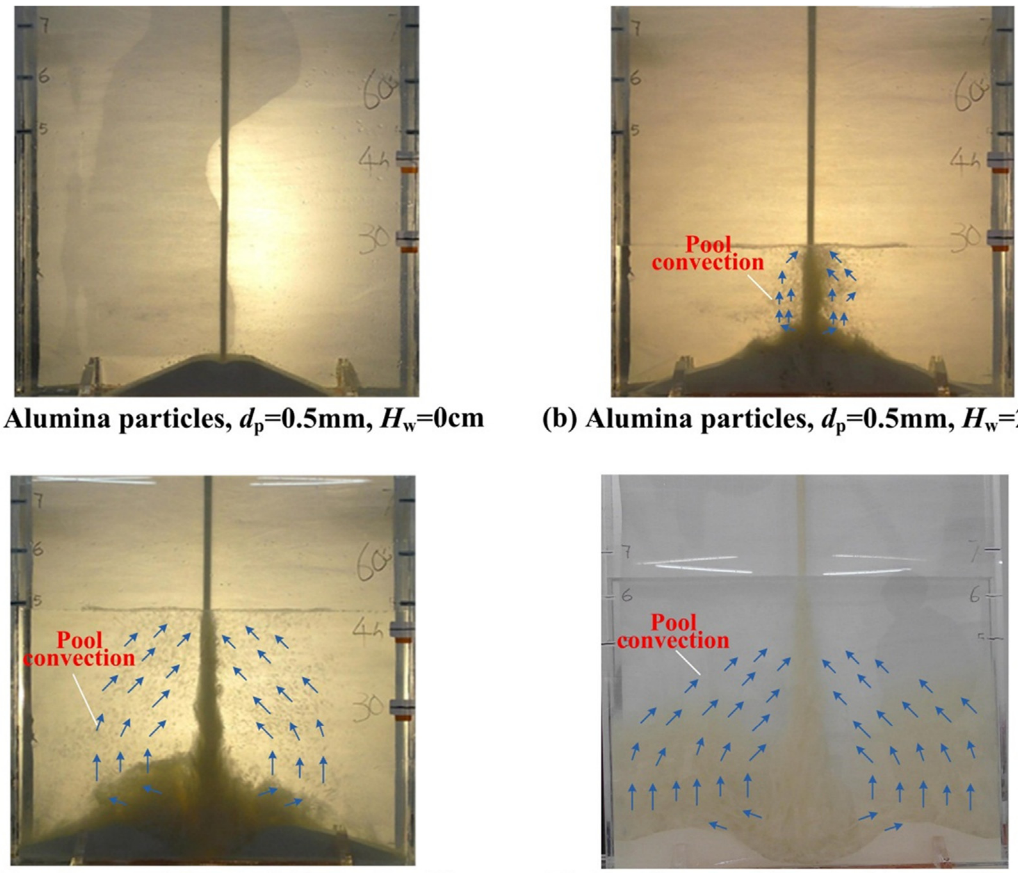

(a) Alumina particles, d_p=0.5mm, H_w=0cm (b) Alumina particles, d_p=0.5mm, H_w=25cm

(c) Alumina particles, d_p=0.5mm, H_w=45cm (d) Alumina particles, d_p=0.5mm, H_w=60cm

Fig. 14. Effect of water depth on pool convection formed (small particles). (Alumina beads, D_{pipe} = 30 mm, H_p =110 cm, W_{tank} = 60 mm).

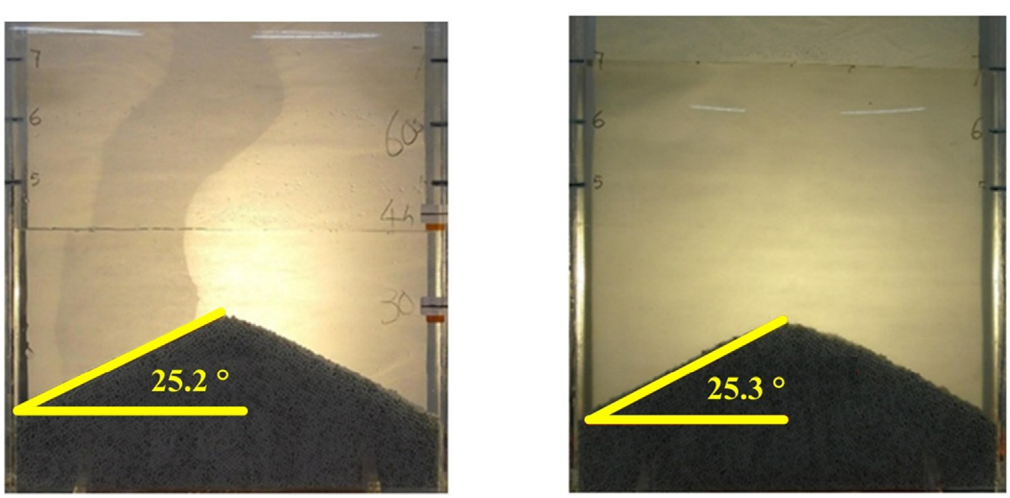

(a) Alumina particles, d_p=6mm, H_w=30cm (b) Alumina particles, d_p=6mm, H_w=60cm

Fig. 15. Effect of water depth on final bed geometry (big particles).

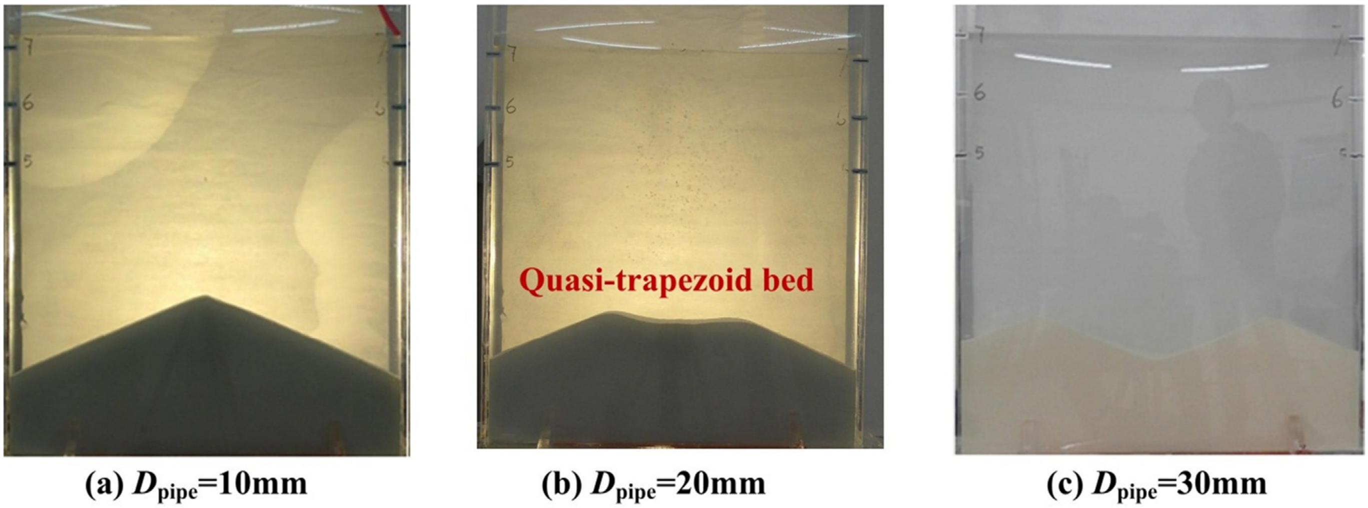

Fig. 16. Effect of particle release pipe diameter on final bed geometry (small particles). (Alumina beads, $d_p = 0.5$mm, $H_w = 60$ cm, $H_p = 110$ cm, $W_{tank} = 60$ mm).

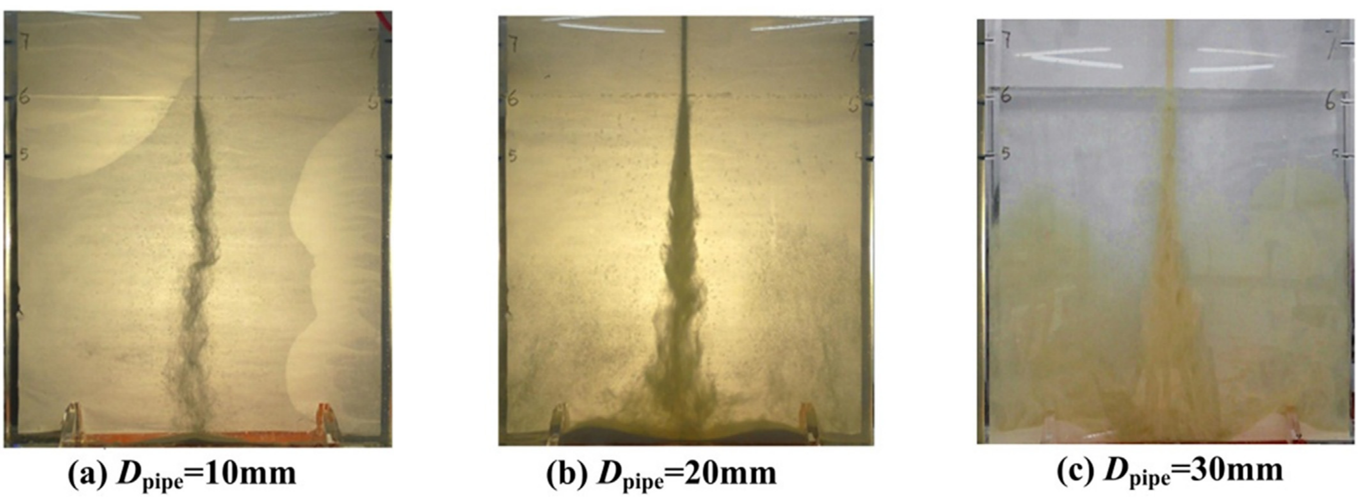

Fig. 17. Effect of particle release pipe diameter on pool convection formed (small particles). (Alumina beads, $d_p = 0.5$mm, $H_w = 60$ cm, H_p =110 cm, $W_{tank} = 60$ mm).

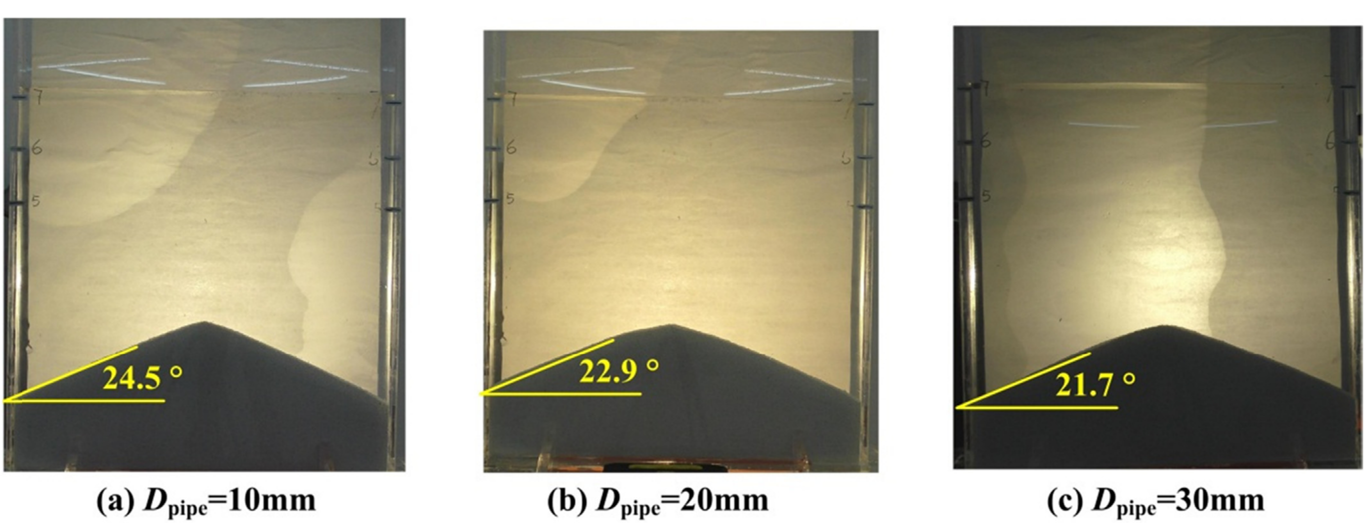

Fig. 18. Effect of particle release pipe diameter on final bed geometry (medium-sized particles). (Alumina beads, $d_p = 2$mm, $H_w = 60$ cm, H_p =110 cm, $W_{tank} = 60$ mm).

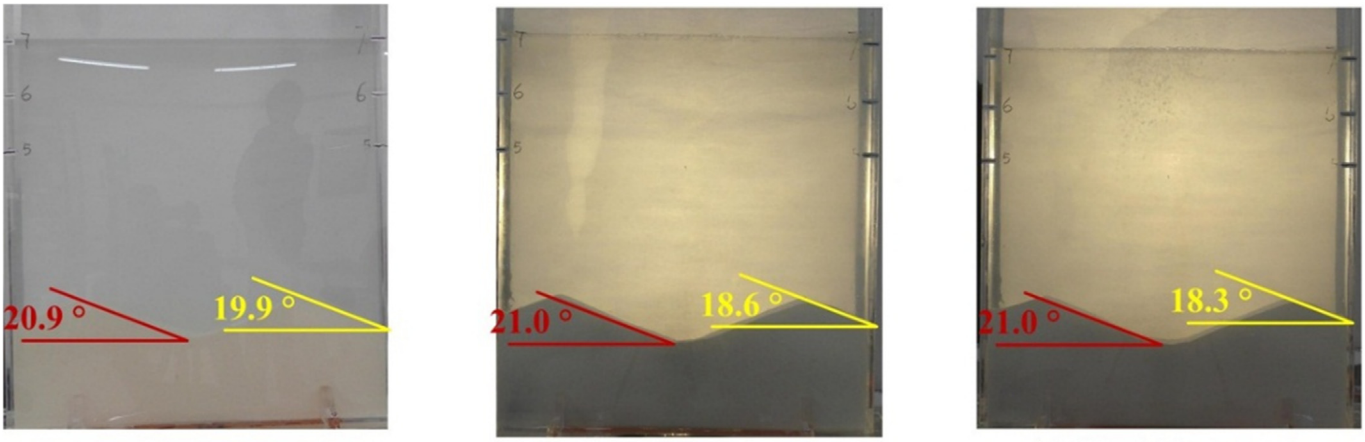

(a) H_p=110cm (b) H_p=120cm (c) H_p=130cm

Fig. 19. Effect of particle release height on final bed geometry for small particles. (Alumina beads, $d_p = 0.5$mm, $H_w = 60$ cm, $D_{pipe} = 30$ mm, $W_{tank} = 60$ mm).

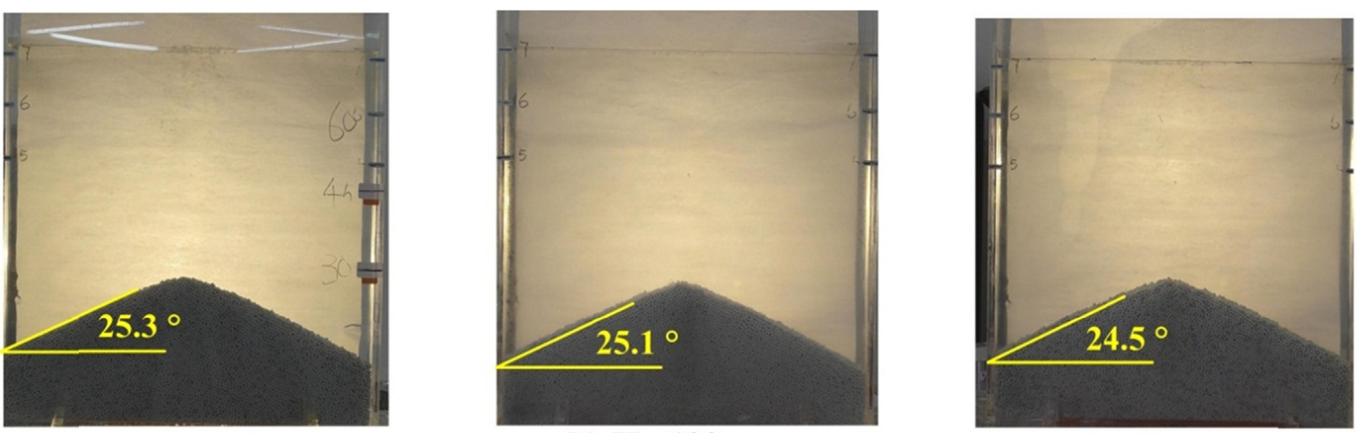

(a) H_p=110cm (b) H_p=120cm (c) H_p=130cm

Fig. 20. Effect of particle release height on final bed geometry for big particles. (Alumina beads, $d_p = 6$mm, $H_w = 60$ cm, $D_{pipe} = 30$ mm, $W_{tank} = 60$ mm).

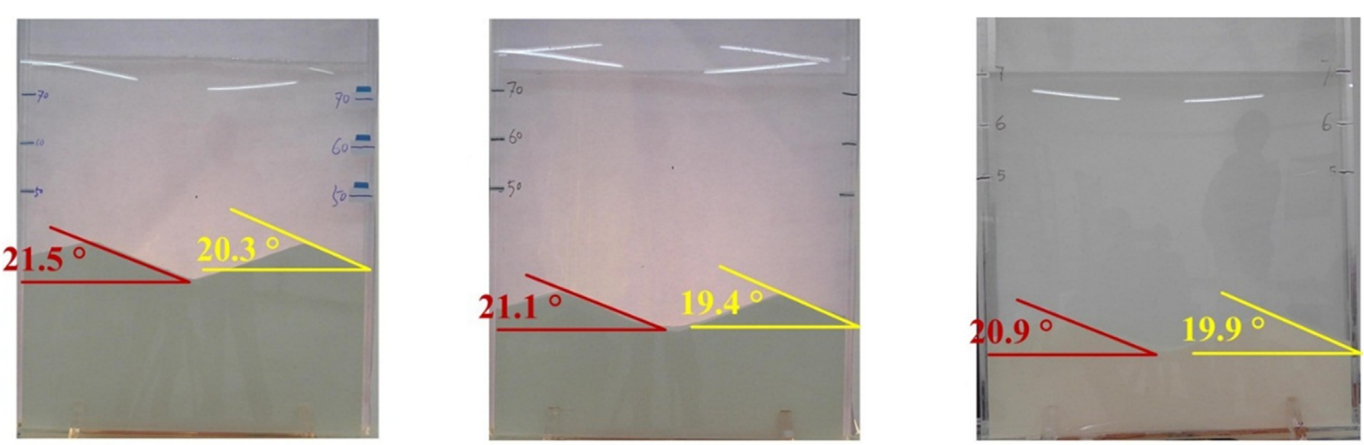

(a) W_{tank}=30mm (b) W_{tank}=45mm (c) W_{tank}=60mm

Fig. 21. Effect of gap thickness of water tank on final bed geometry for small particles. (Alumina beads, $d_p = 0.5$mm, $H_w = 60$ cm, $D_{pipe} = 30$ mm, $H_p = 110$ cm).

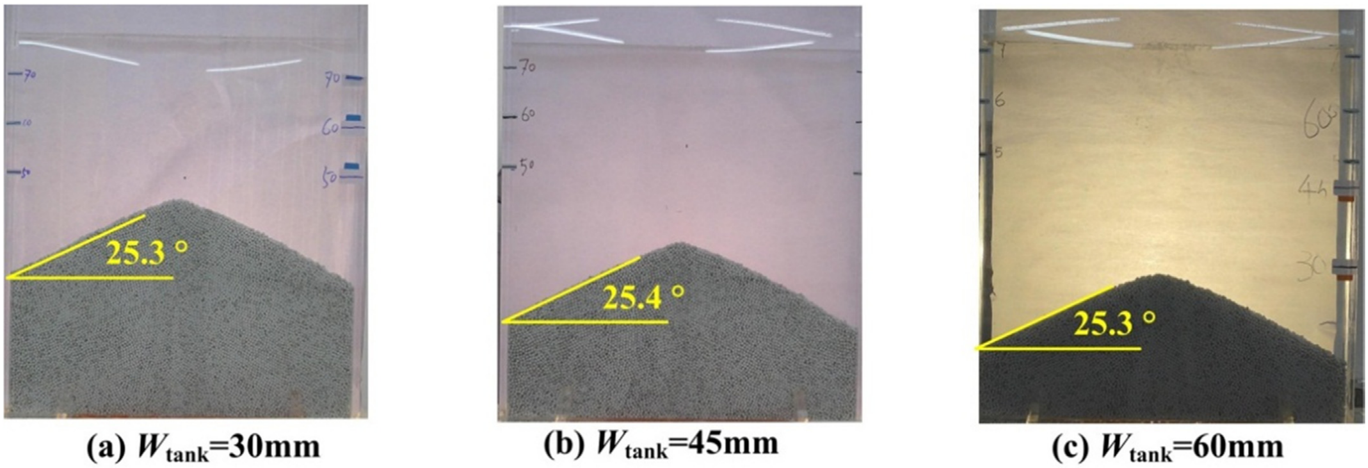

Fig. 22. Effect of gap thickness of water tank on final bed geometry for big particles. (Alumina beads, d_p = 6mm, H_w = 60 cm, D_{pipe} =30 mm, H_p = 110 cm).

to the emergence of particle-inertial dominant regime).

3.2.6. Effect of particle release height

Figs. 19 and 20 illustrate the effect of particle release height on final bed geometry for both smaller particles (0.5 mm) and bigger particles (6 mm). It seems that whatever the regime is, the particle release height seems to have no remarkable influence (with a variation of measured angles less than 2°).

Since theoretically speaking, higher particle release height should result in larger relative velocities between particle flow and the static water pool, leading to more violent pool convection; therefore, it might be deduced that the current change of particle release height (around 20 cm) is still comparatively limited, even comparing to the distance between the particle release device and the bottom of water tank (approx. 150 cm) (see Fig. 4(b)). Nevertheless, based on the mechanisms understood, we can imagine that if the particle release height is sufficiently changed, some difference in final bed geometry or even the regime should be observable, although further elaborate analyses and confirmation might be desired.

3.2.7. Effect of gap thickness of water tank

The effect of gas thickness of water tank on the final bed geometry for both smaller (0.5 mm) and larger particles (6 mm) is depicted respectively in Figs. 21 and 22. It is evident that, except some changes of average bed height caused by the difference in cross-sectional area, no noticeable variation of bed geometry is observable.

To facilitate the experimental operation (e.g. taking out particles), as listed in Table 2, most of our experiments were performed using the water tank with a gap thickness of 60 mm. Even if such a gap thickness is comparatively larger, as compared to others, current analyses suggest that the observed experimental findings in this work should be general characteristics within 2D conditions. In other words, our adoption of water tank with a gap-thickness of 60 mm can achieve a good balance between experimental operations and the reliability of experimental results within 2D conditions.

4. Concluding remarks

Studies on the debris bed formation behavior are important for the improved evaluation of molten-fuel relocation and debris bed coolability. To clarify the mechanisms of this behavior, in this work a series of experiments was performed by discharging various solid particles into two-dimensional water tanks. Based on the experimental observations, it is found that due to the different interaction mechanisms between solid particles and water pool, four kinds of regimes, termed respectively as the particle-suspension regime (flat bed), the pool-convection dominant regime (concave bed), the transitional regime (quasi-trapezoid bed) and the particle-inertial dominant regime (convex bed), are identified. The followed parametric analyses including the final bed geometry as well as the characteristic angles measured suggest that under present experimental conditions the particle size, particle density, particle shape, water depth as well as the particle release pipe diameter are observable to have significant influence on the regimes and final bed geometry formed, while the role of particle release height and gap thickness of water tank seems to be non-remarkable. For future work, studies of empirical-models, especially those predicting the regime transition, might be performed. In addition, in order to provide more confidence for predictive analyses under reactor accident conditions, large-scale three-dimensional experiments might be also conducted. Knowledge and evidence from our experiments would be utilized for the improved design of core catcher as well as the verifications of computer models (esp. the particle-liquid interaction model) in Chinese SFR severe accident analysis codes in the future as well.

Acknowledgments

This work was supported by several research projects in China including the Fundamental Research Funds for the Central Universities (No.15lgjc29).

References

Barabasi, A., Albert, R., Schiffer, P., 1999. The physics of sand castles: maximum angle of stability in wet and dry granular media. Phys. A 266, 366–371.

Cheng, S., Hirahara, D., Tanaka, Y., Gondai, Y., Matsumoto, T., Morita, K., Fukuda, K., Yamano, H., Suzuki, T., Tobita, Y., 2010. Experimental study of bubble behavior in a two-dimensional particle bed with high solid holdup. Xi'an, China, May 17–21, 2010. In: Proc. Of 18th International Conference on Nuclear Engineering (ICONE-18).

Cheng, S., Hirahara, D., Tanaka, Y., Gondai, Y., Zhang, B., Matsumoto, T., Morita, K., Fukuda, K., Yamano, H., Suzuki, T., Tobita, Y., 2011a. Experimental investigation of bubbling in particle beds with high solid holdup. Exp. Therm. Fluid Sci. 35 (2), 405–415.

Cheng, S., Tanaka, Y., Gondai, Y., Kai, T., Zhang, B., Matsumoto, T., Morita, K., Fukuda, K., Yamano, H., Suzuki, T., Tobita, Y., 2011b. Experimental studies and empirical models for the transient self-leveling behavior in debris bed. J. Nucl. Sci. Technol. 48 (10), 1327–1336.

Cheng, S., Yamano, H., Suzuki, T., Tobita, Y., Nakamura, Y., Zhang, B., Matsumoto, T., Morita, K., 2013a. Characteristics of self-leveling behavior of debris beds in a series of experiments. Nucl. Eng. Technol. 45 (3), 323–334.
Cheng, S., Yamano, H., Suzuki, T., Tobita, Y., Gondai, Y., Nakamura, Y., Zhang, B., Matsumoto, T., Morita, K., 2013b. An Experimental investigation on self-leveling behavior of debris beds using gas-injection. Exp. Therm. Fluid Sci. 48, 110–121.
Cheng, S., Yamano, H., Suzuki, T., Tobita, Y., Nakamura, Y., Zhang, B., Matsumoto, T., Morita, K., 2013c. Empirical correlations for predicting the self-leveling behavior of debris bed. Nucl. Sci. Tech. 24 (1), 1–10.
Cheng, S., Matsuba, K., Isozaki, M., Kamiyama, K., Suzuki, T., Tobita, Y., 2014a. An experimental study on local fuel–coolant interactions by delivering water into a simulated molten fuel pool. Nucl. Eng. Des. 275, 133–141.
Cheng, S., Tagami, H., Yamano, H., Suzuki, T., Tobita, Y., Zhang, B., Matsumoto, T., Morita, K., 2014b. Evaluation of debris bed self-leveling behavior: a Simple empirical approach and its validations. Ann. Nucl. Energy 63 (1), 188–198.
Cheng, S., Tagami, H., Yamano, H., Suzuki, T., Tobita, Y., Takeda, S., Nishi, S., Nishikido, T., Zhang, B., Matsumoto, T., Morita, K., 2014c. An Investigation on debris bed self-leveling behavior with non-spherical particles. J. Nucl. Sci. Technol. 51 (9), 1096–1106.
Cheng, S., Matsuba, K., Isozaki, M., Kamiyama, K., Suzuki, T., Tobita, Y., 2015. A numerical study on local fuel-coolant interactions in a simulated molten fuel pool using the SIMMER-III code. Ann. Nucl. Energy 85, 740–752.
Fan, L.S., Zhu, C., 1998. Principles of Gas-Solid Flows. Cambridge University Press, UK.
International Atomic Energy Agency (IAEA), 2016. Fast Reactor Database: 2006 Update. IAEA-TECDOC-1531, IAEA, Austria.
Nakai, R., Suzuki, T., Yamano, H., Seino, H., Ishikawa, H., Kamiyama, K., Koyama, K., Morita, K., 2010. Development of Level 2 PSA methodology for sodium-cooled fast reactors (1) Overview of evaluation technology development. Shanghai, China, October 10–14, 2010. In: Proc. Of 8th International Topical Meeting on Nuclear Thermal-Hydraulics, Operation and Safety (NUTHOS-8).
Ren, L.X., 2015. FR Severe Accident R&D Program. CIAE-cea Associated Laboratory on FR Technology Specialist Meeting 2015. Nov 4, 2015. China Institute of Atomic Energy, Beijing, China.
Tentner, A.M., Parma, E., Wei, T., Wigeland, R., 2010. Evaluation of Design Measures for Severe Accident Prevention and Consequence Mitigation. ANL-GENIV-128. 534 Argonne National Laboratory, Argonne, USA.
Vasilyev, B.A., Shepelev, S.F., Ashirmetov, M.R., Poplavsky, V.M., 2013. BN-1200 reactor power unit design development. Paris, France, March 4-7, 2013. In: International Conference on Fast Reactors and Related Fuel Cycles: Safety Technologies and Sustainable Scenarios (FR-13).
Waltar, A.E., Reynolds, A.B., 1981. Fast Breeder Reactors. Pergamon Press, New York, USA.
Zhang, B., Harada, T., Hirahara, D., Matsumoto, T., Morita, K., Fukuda, K., Yamano, H., Suzuki, T., Tobita, Y., 2010. Self-leveling onset criteria in debris beds. J. Nucl. Sci. Technol. 47 (4), 384–395.
Zhang, B., Harada, T., Hirahara, D., Matsumoto, T., Morita, K., Fukuda, K., Yamano, H., Suzuki, T., Tobita, Y., 2011. Experimental investigation on self-leveling behavior in debris beds. Nucl. Eng. Des. 241 (1), 366–377.